A Self-Oscillating Approach for Wireless Power Transfer

Bhakti Subhash Chowkwale

School of Electrical Engineering

Thesis submitted for examination for the degree of Master of Science in Technology.

Espoo 14.09.2018

Supervisor

Prof. Sergei Tretyakov

Advisors

Dr. Fu Liu

Dr. Prasad Jayathurathnage

Aalto University
School of Electrical
Engineering

Aalto University
School of Electrical
Engineering

Aalto University, P.O. BOX 11000, 00076 AALTO
www.aalto.fi
Abstract of the master's thesis

Author Bhakti Subhash Chowkwale

Title A Self-Oscillating Approach for Wireless Power Transfer

Degree programme Electronics and Nanotechnology

Major Radio Science and Engineering **Code of major** ELEC3038

Supervisor Prof. Sergei Tretyakov

Advisors Dr. Fu Liu, Dr. Prasad Jayathurathnage

Date 14.09.2018 **Number of pages** 45 **Language** English

Abstract

We introduce a robust wireless power transfer scheme that theoretically works for any load and receiver position. We show that capacitive wireless power transfer systems with these new properties can be implemented by modifying simple operational amplifier oscillator circuits. The load and the wireless power link are incorporated into the feedback of the oscillator. The operating frequency adopts to the best possible working condition when the load or receiver position change. We prove the concept by deriving a theoretical model and implementing the same experimentally. The experimentally measured frequency of operation and transferred power agrees well with our analytical solutions.

Keywords Robust Wireless Power Transfer, Self Oscillations, Adaptive Tuning, Capacitive Coupling

Preface

The present work was carried out at the Department of Electronics and Nanoengineering of Aalto University, School of Electrical Engineering.

I would like to thank my supervisor Prof. Sergei Tretyakov for the patient guidance, encouragement and advice he has provided throughout my time as his student. There is still a lot more that I can learn from you. It was a honor for me to work in your group and contribute to its research.

I would also like to thank my advisor Dr. Fu Liu for his patience and advice throughout the thesis. You are always ready to support me in academic and practical matters.

I would like to express my thanks to my advisor Dr. Prasad Jayathurathnage for guiding me in completing my thesis. I appreciate your numerous scientific advices and discussions with you from which I have learnt a lot.

There are several others with whom I would like to express my sincere gratitude to, my colleagues in our research group here at Aalto University for your guidance, assistance and the wonderful time we shared during this period; Mr. Vaaja Matti for his assistance for laboratory equipment and access; and the staff of Sähkopaja Lab for their support and insightful discussions during PCB manufacturing.

Finally, I wish to express my sincere thanks to my family and friends for providing me with continuous encouragement. Without their support it would have been difficult to finish this thesis. Thank you.

This work was supported by the European Unions Horizon 2020 research and innovation programme - Future Emerging Topics (FETOPEN) under grant agreement No 736876.

Otaniemi, 14.09.2018

Bhakti Subhash Chowkwale

Contents

List of Figures

Symbols and Abbreviations

Symbols

$\pm V_{\mathrm{CC}}$	Source voltage

Abbreviations

CPT	Capacitive Power Transfer
IPT	Inductive Power Transfer
Op-amp	Operational Amplifier
WPT	Wireless Power Transfer

1 Introduction

Wireless Power Transfer (WPT) has been a topic for research ever since Nikola Tesla discovered the possibility of transmitting power wirelessly in the early 20th century [1]. Up until Brown's demonstration of the first wireless power transfer system in 1963, there was a lack of mature radio frequency technology [2]. Ever since, there has been a significant improvement in the field due to which we can find the use of wireless power transmission in applications such as consumer electronics [3], electric vehicle charging [4], biomedical implants [5, 6], industrial applications, etc. As the name suggests, wireless power transfer is the ability to transmit power without a physical wired connection between the power source and receiver. Based on the technology used, near-field wireless power transfer can be broadly categorized into two types, Inductive Power Transfer (IPT) and Capacitive Power Transfer (CPT). IPT uses magnetic coupling between two coils and energy is delivered from the primary coil (connected to the source) to the secondary coil (connected to the load). Whereas in CPT, coupling is between two pairs of metallic plates that act as parallel-plate capacitors. For our implementation, we shall exploit CPT for power transfer.

A typical WPT system has three distinct sections, namely, the microwave generator, the transmitter, and the receiver. The utility power is converted to microwave power by using a generator since DC or 50-60 Hz power cannot be effectively transferred via free space [7]. Optimal power transfer occurs when microwave generator frequency is equal to the self-resonant frequency of the transmitter-receiver system, and the input impedance of the system is matched to the generator. In practice, however, the variations in load impedance and coupling are probable, leading to derailment of the system from optimal operation. The system needs to be tuned continuously to achieve frequency and impedance matched conditions. One method is by introducing additional impedance tuning circuit. Another method to tackle this problem is integrating the three distinct sections of a general WPT to one system. This can be achieved by designing a self-oscillating scheme wherein the generator, transmitter, receiver and load are incorporated into one circuit. A robust system which has the ability to operate in the most favorable operating regime without additional tuning while the system is undergoing variations is necessary. This is a crucial performance criterion for WPT systems.

The goal of this thesis is to introduce the concept and experimental validation of self-oscillating WPT technique which is the new paradigm for WPT. We will concentrate on CPT and methods to improve its performance based on the following aspects: the power delivered to the load and the robustness of operation due to changes in load and receiver position. The structure of the thesis is as follows: Chapter 2 gives the background of WPT techniques and introduces the current approach. It also provides an insight on basics of operational amplifiers and the RC oscillator theory. Chapter 3 focuses on a particular WPT design within the new paradigm. The theoretical analysis and experimental validation of the design (operating frequency and robustness against the load and coupling variations) are provided. Chapter 4

describes an alternative self-oscillating WPT design using Colpitts oscillator along with the experimental results. Chapter 5 concludes the thesis with a brief summary of our work along with a discussion of our future plan on improving the system performance.

2 Background

A wireless power device is capable of being powered remotely. WPT enables devices to be compact because the device does not require large batteries [8, 9]. Therefore, WPT technology is very important. Wireless power transfer can be classified into two main categories, non-radiative (near field) power transfer and radiative (far field) power transfer depending on the distance of energy transfer [10]. Non-radiative WPT relies on the near-field (magnetic or electric) coupling for power transfer. It operates at a distance less than the wavelength of the transmitted signal [11]. While in radiative WPT, power is emitted from an antenna and propagates through a medium over long distances (i.e. larger than the working wavelength) in the form of an electromagnetic wave. An overall classification of the WPT techniques can be found in Figure 2.1.

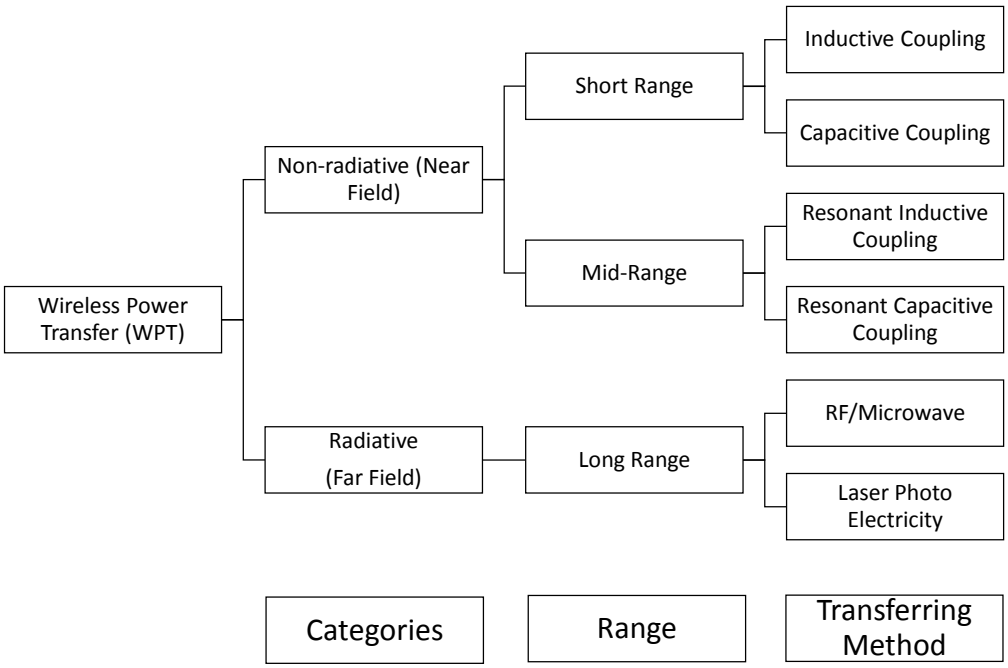

Figure 2.1: Classification of WPT based on categories, range and transferring method.

The key performance parameters for applications include system level performance characteristics, such as transferred power (TP) and application level requirements such as transfer distance, misalignment tolerance and load variation. TP refers to the output power at the load [12] and is affected by application level requirements as the system is sensitive towards such parameters. We require a high value of TP indicating a high power delivery to the load, but load variation and misalignment lead to the WPT system's degraded performance. In this thesis, we will introduce a new paradigm for WPT named self-oscillating WPT which enables us to deliver optimal power to the load regardless of the load variation, transfer distance and the misalignment of the transmitter and receiver.

The chapter outline is as follows: Section 2.1 discusses the operating principle of WPT in the short and mid-range regimes. Section 2.2 describes the behavior of general WPT schemes and their robustness against variations of system parameters such as the load, operating frequency, coupling between the transmitter and receiver and adaptive tuning properties. Section 2.3 introduces the concept of self-oscillation and shows how it can be used to construct a robust WPT system. Section 2.4 describes the basics of operational amplifiers and Section 2.5 discusses the basic RC oscillator. Section 2.6 explains the conventional WPT scheme and in Section 2.7 we showcase the transition from the conventional WPT scheme to the self-adaptive scheme.

2.1 Operating Principle of WPT

Inductive and capacitive couplings are two WPT techniques to transmit power using electromagnetic fields. The ability to transmit power depends on the mutual inductance, M, or mutual capacitance, C. The values of M and C, depending on the distance between the transmitter and receiver, define the categories and range in Figure 2.1. We concentrate on the non-radiative region, where practical amounts of power can be transferred by capacitive or inductive coupling techniques. The following discussion introduces inductive and capacitive coupling techniques.

Inductive power transfer (IPT) [13, 14] and capacitive power transfer (CPT) [15] are two methods to transmit power without a physical wired connection. IPT uses coupled inductive coils to transmit energy through magnetic field [16, 17]. This has been widely used for charging portable electronic devices [18] and electric vehicles [19]. On the other hand, CPT transfers power via capacitive coupling between parallel-plate capacitors acting as the transmitter and receiver. Compared to IPT [20], CPT is not well developed yet. However, it is developing rapidly and has already been used in applications [21, 22]. Currently, CPT systems are widely implemented with the help of a series inductor. However, such setup utilizes a large coupling capacitor or a high switching frequency. Such a system can be implemented with a non-resonating design with one constraint being the value of the coupling capacitance should be in the nF range [15].

As an example, let us discuss the operating principle of IPT. As we know, IPT is the power transfer between coils (the transmitter and receiver) by magnetic field. An alternating current through the transmitter creates an oscillating magnetic field according to Ampere's law. The magnetic field then couples to the receiver, where it induces an alternating voltage, following Faraday's law. This voltage is connected to the load directly or is connected to a rectifying circuit. As a result of this voltage, a current is generated at the receiver. Similarly, the same concept can be used for CPT, but instead of magnetic field we have electric fields [19].

2.2 Robustness Against System Parameters

Many parameters such as the load resistance, frequency of operation, coupling between the transmitter and receiver, etc. define the system performance. Change in any one of these parameters leads to variation in power transferred from the transmitter to receiver. The optimal power transfer happens when the load impedance is matched to the source impedance. However, the load impedance is a function of the coupling coefficient, therefore it is necessary to satisfy the matching condition at transmitter and receiver simultaneously in order to achieve optimal power transfer. Most studies consider the ideal case to be when the transmitter and receiver are aligned [23]. However, in reality misalignment between the two cannot be avoided leading to a decline in power transfer [24, 25]. This results in the decrease of robustness of the system as it is not immune to changes in alignment of the system. Power transfer is maximum when the coupling is strong and there is no misalignment, but once misalignment is introduced, it decreases coupling which leads to a reduction in power received at the load. In practical applications, misalignment is highly inevitable, leading to deviations from the optimal performance [26]. This is an indication of a less robust system. In addition to misalignment, variations of load resistance also decrease the performance of the system. The optimal load resistance is used to design the system, but in reality it is not easy to ensure operation at the optimal load. The value of the load is application dependent [27]. For example, consider the application of battery charging. The load in this case is the battery charging circuit. When the battery has less charge, the current drawn by the system is high. This results into a low load resistance. But, when the battery is almost charged, the amount of current drawn by the system is low, indicating a high load resistance.

Therefore, there is a necessity to design robust WPT systems that can adapt to keep up with changes in environment and transmitter-receiver movements. Adaptive systems were designed to maintain good performance regardless of the mismatch. They can be classified into systems that are implemented by adjusting the source frequency and tuning the impedance of the transmitter or receiver [28]. In [29], digitally tuned capacitors were used to adjust the operating frequency maintaining excellent matching at small distances. But, they were not able to obtain optimum matching for larger distances limiting the system use. Therefore, to realize a system which can transmit power effectively regardless of the variations (or mismatch) is difficult. Thus, attaining an adaptive wireless power scheme which can adjust to its surrounding became an important area of research.

Recent developments demonstrate that parity-time symmetric WPT systems can be robust against coupling variations within the strong coupling region [30, 31], but realization of negative resistance using impedance inverters or other means is inherently a low-efficiency process [7, 30]. In papers [31–33], our group has theoretically proposed a generic on-site WPT scheme, which ensures operation robustness by generating oscillations directly at the load itself and does not suffer from the low efficiency of negative-resistance circuits.

2.3 Introduction to Self-Oscillation

There are certain conditions under which oscillations occur in a system. Let us first discuss the basic oscillator theory followed by the concept of self-oscillations.

Basic Oscillator Theory A basic block diagram of an oscillator circuit can be found in Figure 2.2.

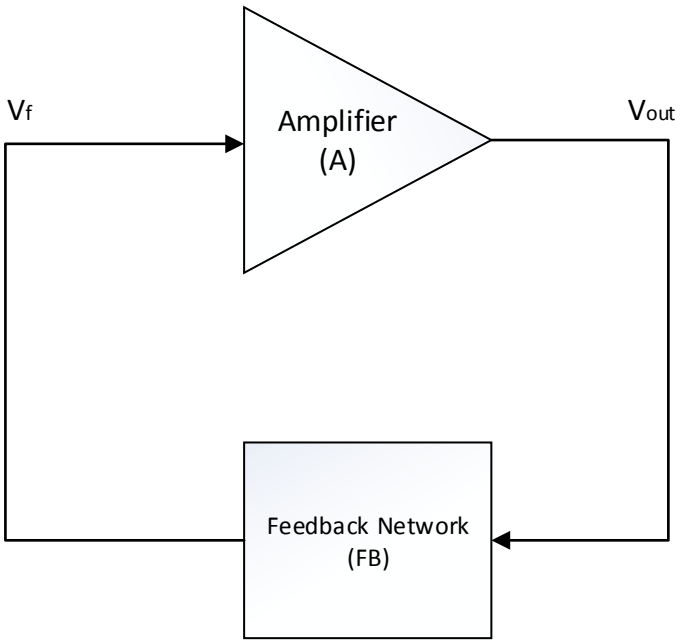

Figure 2.2: Basic block diagram of oscillating system.

To understand how to design a basic oscillating circuit, let us first discuss the criteria necessary for oscillation. We need to ensure that Barkhausen's criterion is obeyed for oscillations. This criterion is the mathematical condition that needs to be satisfied in order to define whether an electronic circuit will oscillate or not [34]. It consists of two conditions, first, there must be positive feedback or regenerative feedback to the input terminals. The feedback network provides a phase shift of 180° and the amplifier provides a phase shift of 180°, equaling 360°. This means that the phase shift between the output terminal (V_{out}) and input terminal (V_{f}) is a multiple of 2π. Secondly, the absolute loop gain must be equal to 1, i.e. $|\text{A}\times\text{FB}|=1$.

Barkhausen's criterion is used to design oscillators for electronic circuits. The oscillator usually consists of operational amplifiers or transistor amplifiers connected in a feedback loop to provide positive feedback. Oscillators convert DC voltage to an AC output. As a result, oscillators are found in many RF system applications. WPT is an example where microwave power generators are used. Such WPT systems consist of a transmitter, receiver, and a load. But, we face a problem of power

losses due to many lossy components in each stage. However, this problem can be approached by using the concept of self-oscillating WPT systems where the number of lossy components is largely reduced.

Self-Oscillating WPT In the self-oscillating WPT systems, the load resistance is present in the feedback loop, making it an integral part of the system. In this thesis, we discuss this new paradigm for WPT in which the entire system, i.e. transmitter, receiver and the space in between, forms a unified microwave power generator. The load becomes a part of the oscillating system. As the oscillations are directly generated at the receiver regardless of the parameter variations, there is no need for additional tuning. This results in a robust WPT system operating for a wide range of receiver positions C_{p} and load resistances R_{L} [31–33]. A general schematic of a self-oscillating WPT system is shown in Figure 2.3.

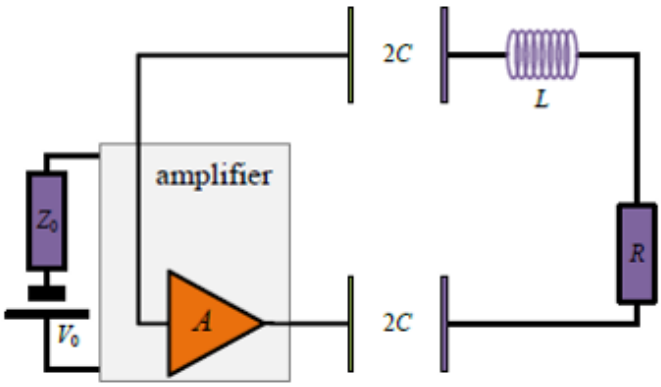

Figure 2.3: Circuit schematic of the general concept of self-oscillating WPT.

As the oscillations are generated at the load in this self-oscillating WPT system, if there is no load, there is no oscillation. Also, the operating frequency is automatically adopted to the optimal working condition under the changes of load and receiver positions (misalignment and transfer distance) [31–33].

2.4 Operational Amplifiers

In this thesis we will use operational amplifiers (op-amp) to implement the self-oscillating WPT circuit. The op-amp is a device extensively used for amplification purposes in signal generation, filtering and basic mathematical or logical operations. Op-amps are three-terminal devices, with two input terminals, namely the inverting terminal (usually denoted by a "-" sign) and the non-inverting terminal (usually denoted by a "+" sign). The output terminal sources voltage or current but, for our application we will be using voltage based op-amps. The output voltage of the op-amp depends on the gain defined by the components in the circuit multiplied by

the difference between the voltages applied at the input terminals. Using op-amps, we can generate oscillating voltages of different patterns such as sinusoidal, square, sawtooth or triangular that operate at different frequencies. Few terms related to op-amps used in this thesis are discussed next.

Output Voltage Swing The output voltage swing of an amplifier is defined as the peak to peak voltage at the output of the amplifier. The output of the op-amp is limited by the supply voltages, but due to the internal structure of the op-amp, the op-amp produces an output voltage less than the supply voltage. This drop in voltage is usually mentioned in the datasheet of the op-amp.

Slew Rate The slew rate of an op-amp is an important parameter we should consider while working for oscillation purpose. Slew rate defines how fast the output voltage can change due to a change in input and is measured in V/μs. Therefore, it defines the highest possible frequency of operation of the op-amp. The relation between the slaw rate (SR) and the maximum working frequency $f_{\max}$ is formulated as

$$\mathrm{SR} = 2\pi f_{\max} V_{\mathrm{p}} \tag{2.4.1}$$

where V_{p} is the peak amplitude of the output signal. Using this formula we can calculate the slew rate needed for the operation of our circuit and choose the proper op-amp. In our self-oscillating circuits for WPT purpose, square waveforms are expected from the output terminal. However, in the limiting case when the op-amp operates at a frequency close to $f_{\max}$, the output of the op-amp is affected. First of all, the waveform becomes trapezoidal instead of square shape. Secondly, the amplitude of the output can be decreased. These occur due to the op-amps inability to keep up with the changes at the input. The internal circuit diagram of the op-amp shows that the slew rate limitations occur due to the rate at which the internal coupling capacitor of the op-amp charges and discharges [35].

Buffer Circuit Buffers are also known as voltage follower circuits with unity gain. It will give the input voltage at the output, but change the impedance from high to low. This is very helpful when we measure voltage across high impedance loads. As the impedance of the oscilloscope probe is 1 MΩ, while measuring values higher than this, the impedance viewed by the oscilloscope will not be isolated from high values of the resistor. Therefore, in order to isolate the oscilloscope probe and the measurement points, a buffer circuit is used.

Tank Circuit The resonant circuit or LC circuit consists of an inductor and capacitor which stores energy. LC circuits are used for generating signals at a particular frequency or as filters.

2.5 Basic RC Oscillator

We first discuss a typical RC oscillator illustrated in Figure 2.4 which we will use to construct our WPT circuit. In this RC oscillator circuit, the reference voltage V_{r} at the non-inverting terminal is set by the voltage divider circuit using R_1 and R_2, i.e.,

$$V_{\mathrm{r}} = \beta V_{\mathrm{out}} \tag{2.5.1}$$

with

$$\beta = \frac{R_2}{R_1 + R_2} \tag{2.5.2}$$

At the inverting terminal, the feedback path for this circuit is through the resistor R_{f} and capacitor C_0. The charging and discharging of the capacitor C_0 affects the voltage at V_1. The competition between V_1 and V_{r} results to the output switching between $+V_{\mathrm{CC}}$ and $-V_{\mathrm{CC}}$. When V_{r} is larger (smaller) than V_1, the output is $+V_{\mathrm{CC}}$ $(-V_{\mathrm{CC}})$. If we assume the op-amp here is ideal which has infinite input resistance, zero output resistance, and infinite slew rate, the time period of this oscillator is

$$T = 2\tau \ln \frac{1+\beta}{1-\beta} \tag{2.5.3}$$

where

$$\tau = R_{\mathrm{f}} C_0 \tag{2.5.4}$$

is the time constant. The oscillation frequency is then simply $f = 1/T$. This analysis will help us to define operating conditions for the conventional WPT system.

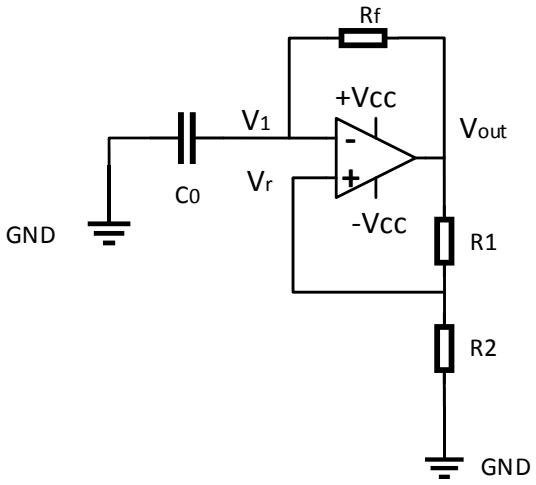

Figure 2.4: Basic RC oscillator circuit.

2.6 Conventional WPT Circuit

A conventional WPT circuit consists of an oscillating circuit with a WPT unit connected to it. Figure 2.5 shows a simple example, in which we can see that the

basic RC oscillator operates as a generator, and the WPT unit transfers energy to the load wirelessly. In the conventional WPT system, the WPT unit does not affect the operating frequency of the generator as it is independent. The two capacitors C_{p} form the wireless power link and R_{L} is the load resistance. The parallel-plate capacitors C_{p} can be manufactured using two pairs of metal sheets. The change in the distance or the overlap area between the two sheets leads to the change in capacitance, which follows the formula:

$$C_{\mathrm{p}} = \frac{\epsilon_0 \epsilon_{\mathrm{r}} A}{d} \tag{2.6.1}$$

where ϵ_0 is the permittivity of free-space, ϵ_{r} is the relative permittivity of the material between the sheets, A is the overlap area of the plates and d is the distance between the two plates.

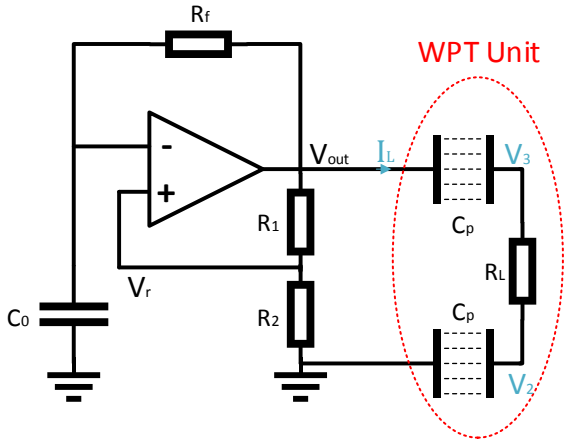

Figure 2.5: Conventional capacitive WPT system.

The current flowing through the WPT unit, i.e., $C_{\mathrm{p}} - R_{\mathrm{L}} - C_{\mathrm{p}}$, is identical (Kirchoff's current law) which gives

$$I_{\mathrm{L}} = C_{\mathrm{p}} \frac{\mathrm{d}(V_{\mathrm{out}} - V_3)}{\mathrm{d}t} = \frac{V_3 - V_2}{R_{\mathrm{L}}} = C_{\mathrm{p}} \frac{\mathrm{d}V_2}{\mathrm{d}t} \tag{2.6.2}$$

From this equation, we quickly get that the voltage drop across the capacitors C_{p} are always the same, i.e.,

$$V_{\mathrm{out}} - V_3 = V_2 \tag{2.6.3}$$

The operation of this WPT system can be solved analytically with proper initial conditions. The initial conditions can be determined using the circuit simulation tool LTSpice. Figure 2.6 shows the voltage oscillations from simulation, the green waveform is the output of the op-amp measured at V_{out}, the blue waveform is obtained at V_3 and the red waveform at V_2.

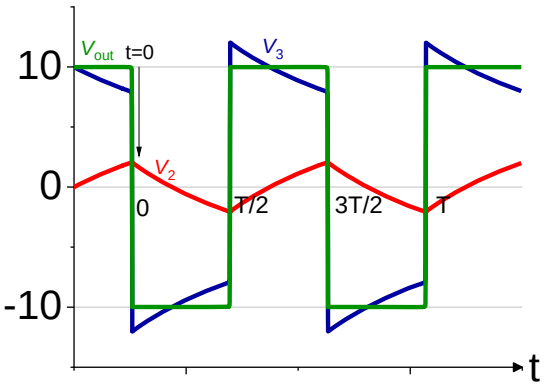

Figure 2.6: Voltage oscillations versus time and the initial conditions at time $t = 0$.

If we consider the initial conditions at $t = 0$ when the output is switching from $+V_{CC}$ to $-V_{CC}$, as shown in Figure 2.6, the initial conditions can be written as,

$$\begin{aligned} V_2(0) &= V_{20} \\ V_3(0) &= -V_{CC} - V_{20} \end{aligned} \tag{2.6.4}$$

Using the initial conditions and solving Equation 2.6.2 we obtain the functions for the voltages $V_{3\,\mathrm{down}}(t)$ and $V_{2\,\mathrm{down}}(t)$ for $0 < t < T/2$:

$$V_{3\,\mathrm{down}}(t) = -\frac{V_{CC}}{2} - \frac{1}{2}(2V_{20} + V_{CC})e^{\frac{-2t}{C_p R_L}} \tag{2.6.5}$$

$$V_{2\,\mathrm{down}}(t) = -\frac{V_{CC}}{2} + \frac{1}{2}(2V_{20} + V_{CC})e^{\frac{-2t}{C_p R_L}} \tag{2.6.6}$$

As the behavior of the circuit during $0 < t < T/2$ and $T/2 < t < T$ is symmetric, we have $V_{2\,\mathrm{down}}(T/2) = -V_{20}$. Therefore, the constant V_{20} can be obtained from this equation which gives

$$V_{20} = \frac{1}{2} V_{CC} \tanh\left[\frac{T}{2C_p R_L}\right] \tag{2.6.7}$$

where T is the oscillating period given by Equation 2.5.3. With these functions for voltages across the load, the average power delivered to the load P_{avg} can be determined by the using the formula

$$P_{avg} = \frac{2}{T}\int_0^{T/2} \frac{(V_{3\,\mathrm{down}}(t) - V_{2\,\mathrm{down}}(t))^2}{R_L} \mathrm{d}t \tag{2.6.8}$$

Substituting the derived voltage equations into the power equation, we obtain

$$P_{avg} = \frac{V_{CC}^2}{R_L} \frac{2C_p R_L}{T} \tanh\left(\frac{T}{2C_p R_L}\right) \tag{2.6.9}$$

To compare the performance of this conventional WPT system to that of a wired connection, we utilize the reference power value $P_0 = V_{CC}^2/R_L$, which defines the

power delivered to the load when the load is directly connected to the power supply. The performance parameter P_r is then defined as the ratio of the average delivered power P_{avg} to P_0 in the wired scenario:

$$P_r = \frac{P_{avg}}{P_0} = \frac{2C_pR_L}{T} \tanh\left(\frac{T}{2C_pR_L}\right) \tag{2.6.10}$$

where period T is given by Eq. 2.5.3. The aim is to deliver the maximum possible power to the load comparable to the wired scenario. This can be achieved by varying the capacitors C_p and load resistance R_L. The power ratio P_r as a function of these two parameters can be observed in Figure 2.7. To plot the P_r relationship, we set $C_0 = 1$ nF, $R_f = 50$ kΩ, and $\beta = 0.2$.

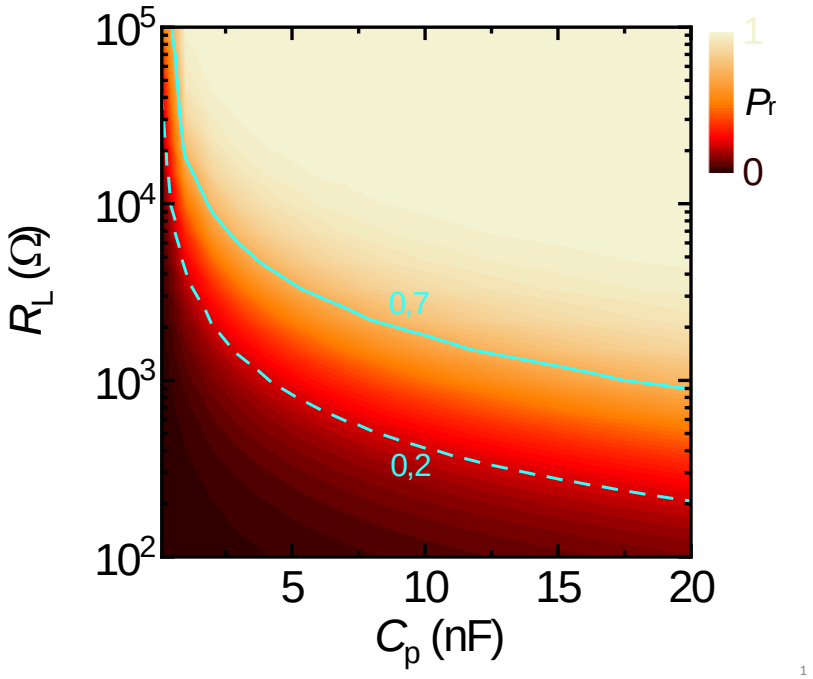

Figure 2.7: Color map of P_r as a function of C_p and R_L.

From Figure 2.7, we can observe that as C_p and R_L increases, P_r increases. It means that if we want WPT operation comparable to wired connection, we need to use high values for C_p and R_L. The light yellow shade shows possible combinations for maximum P_r. We can also observe that, for resistance values smaller than 20 kΩ, the power ratio is poor. This is due to very quick discharging of C_p (smaller resistance allows larger current) thus making the operation limited to only high values of load resistance.

Our discussion till now was focused on the power delivered to the load. This is one of the most crucial aspects of WPT systems, but due to the design of the system, there is a considerate amount of overall power loss. Typical WPT systems

are brought to resonance to realize efficient power transfer. The coupled-antenna mode (CPT or IPT) is optimized to reduce radiation into the surrounding space. In conventional models, modification of the receiver position or of its electromagnetic properties results in the necessity of dynamically tuning the whole system to restore the resonant matching condition. It implies poor robustness to the receiver location and load impedance, as well as additional energy consumption in the control network.

2.7 Transition from Conventional WPT System to New WPT Paradigm

A general transition from the conventional system to the new paradigm is illustrated in Figure 2.8. To implement our concept of self-oscillating WPT, we modified the position of the WPT unit. Instead of keeping the WPT unit independent as in conventional WPT systems, as shown in Figure 2.8 A, we integrate it into the feedback of the oscillator circuit, as shown in Figure 2.8 B.

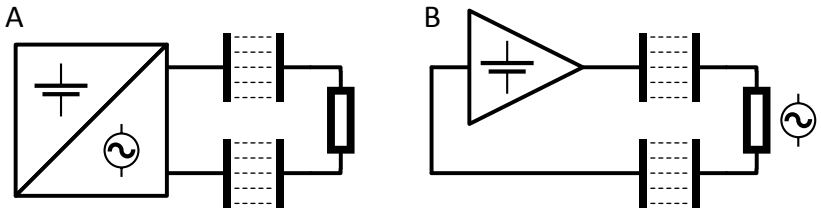

Figure 2.8: Transition from conventional WPT system to new paradigm.

The new paradigm for WPT can be implemented using the RC oscillator discussed above. There are two methods for this implementation.

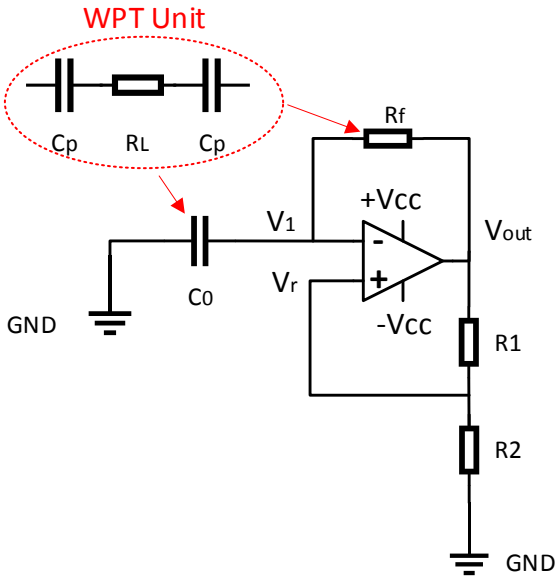

Figure 2.9: Implementation possibilities of new WPT paradigm.

Using Figure 2.9 as a reference, the WPT unit can be substituted in place of C_0 or R_f. Let us discuss each possibility in the following chapter. The next chapter introduces our example of the self-adaptive technique for WPT. The general concepts discussed here will be used in the analysis of the self-adaptive approach.

3 A Self-Adaptive Approach for WPT

The self-adaptive approach for WPT is based on the self-oscillating WPT paradigm discussed in [31–33]. It is a robust on-site WPT system that automatically adjusts itself to the optimal regime although the load resistance and the receiver position vary in a broad range. In Section 3.1, we discuss the analytical solution for the system. Then the experimental demonstration using lumped elements and parallel plates for the WPT unit are provided in Sections 3.2 and 3.3. In Section 3.4, we study the other possible position of the WPT unit and show that it is less favorable and leads to higher power losses.

3.1 Analytical Solution for Self-Adaptive Approach

In Section 2.7, we introduced possibilities for integrating the WPT unit in an RC oscillator. This self-adaptive solution is implemented by substituting the WPT unit in place of the feedback resistor R_f in Figure 2.9, as shown in Figure 3.1.

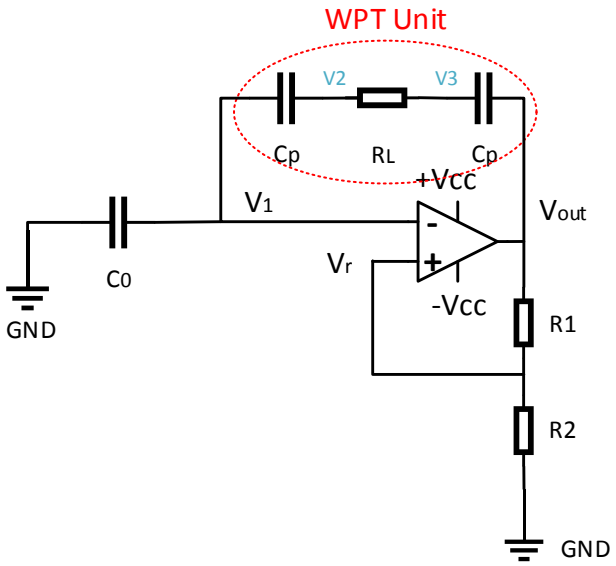

Figure 3.1: Circuit diagram for self-adaptive WPT approach.

The derivation for the time period of oscillations and power delivered to the load is as follows. Let us consider the feedback path which includes our WPT unit $C_\mathrm{p}-R_\mathrm{L}-C_\mathrm{p}$. We know that the same current i flows through all these components in the feedback path. Under the assumption of ideal op-amp, the current does not flow into the input terminal of the op-amp due to high input resistance, but it flows through C_0 to the ground. Expressing this in terms of mathematical equations we get

$$i = C_\mathrm{p}\frac{\mathrm{d}(V_\mathrm{out}-V_3)}{\mathrm{d}t} = \frac{V_3-V_2}{R_\mathrm{L}} = C_\mathrm{p}\frac{\mathrm{d}(V_2-V_1)}{\mathrm{d}t} = C_0\frac{\mathrm{d}V_1}{\mathrm{d}t} \tag{3.1.1}$$

The output of the op-amp will switch between the power supply rails based on the following conditions:

$$V_{\text{out}} = \begin{cases} +V_{\text{CC}} & V_{\text{r}} > V_1 \\ -V_{\text{CC}} & V_{\text{r}} < V_1 \end{cases} \tag{3.1.2}$$

From Equation 3.1.1, we can quickly get two relations: one is the same voltage drop across two C_{p}, i.e. $V_{\text{out}} - V_3 = V_2 - V_1$, which gives:

$$V_3 = V_{\text{out}} - V_2 + V_1 \tag{3.1.3}$$

and the second one is the relation between voltages V_2 and V_1

$$V_2 = \frac{C_{\text{p}} + C_0}{C_{\text{p}}} V_1 \tag{3.1.4}$$

We will follow the same procedure as in the case of conventional WPT system to find the solution. The initial conditions can be defined with the help of Figure 3.2 obtained using LTSpice. The output is shown by the green trace, V_3 by the blue trace and V_2 by the red trace.

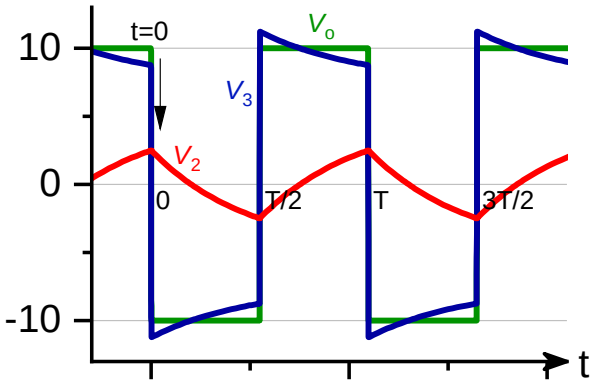

Figure 3.2: Voltage oscillations versus time and the initial conditions at $t = 0$ of the self-adaptive WPT system.

We take the time $t = 0$ when the output switches from $+V_{\text{CC}}$ to $-V_{\text{CC}}$. At an instant right before $t = 0$, the voltage conditions at each node are as follows:

$$\begin{aligned} V_{\text{out}} &= V_{\text{CC}} \\ V_1 &= \beta V_{\text{CC}} = V_{\text{r}} \\ V_2 &= \tfrac{C_{\text{p}}+C_0}{C_{\text{p}}} V_1 \end{aligned} \tag{3.1.5}$$

However, at an instant right after $t = 0$ when the output of the op-amp switches its state from $+V_{\text{CC}}$ to $-V_{\text{CC}}$, the voltages are changed to the following:

$$\begin{aligned} V_{\text{out}} &= -V_{\text{CC}} \\ V_1 &= \beta V_{\text{CC}} \\ V_2 &= \tfrac{C_{\text{p}}+C_0}{C_{\text{p}}} V_1 \end{aligned} \tag{3.1.6}$$

V_1 and V_2 maintain their states as there is charge accumulation in the capacitors. At the same time, V_3 will follow the change of V_{out} to satisfy Equation 3.1.3. Using these conditions and the relationship between V_1, V_2 and V_3 in 3.1.3, we are able to solve 3.1.1 and achieve the analytical solutions

$$V_{1\,\text{down}}(t) = \frac{V_{\text{CC}}}{2C_0 + C_\text{p}} \left[(C_\text{p} + 2C_0\beta + C_\text{p}\beta)e^{-t/\tau} - C_\text{p} \right] \tag{3.1.7}$$

$$V_{3\,\text{down}}(t) = -\frac{V_{\text{CC}}}{2C_0 + C_\text{p}} \left[(C_\text{p} + 2C_0\beta + C_\text{p}\beta)e^{-t/\tau} C_0/C_\text{p} + C_\text{p} + C_0 \right] \tag{3.1.8}$$

where $\tau = C_0 C_\text{p} R_L/(2C_0 + C_\text{p})$ is the characteristic time. $V_{2\,\text{down}}(t)$ can be also obtained from Equation 3.1.4. These solutions are for the first half of the period $0 < t < T/2$. When $t = T/2$, the switching condition $V_1 = V_\text{r}$ is satisfied again and the output will switch. The analytical solutions for the second half period $T/2 < t < T$ can be obtained simply by

$$\begin{array}{rcl} V_{2\,\text{up}}(t - T/2) & = & -V_{2\,\text{down}}(t) \\ V_{3\,\text{up}}(t - T/2) & = & -V_{3\,\text{down}}(t) \end{array} \tag{3.1.9}$$

where $V_{2\,\text{up}}(t)$ and $V_{3\,\text{up}}(t)$ are the solutions of WPT system from $T/2$ to T. This is because the circuit has symmetric operation in both half cycles of the waveform. To calculate the period from the analytical solution we need to observe the change in V_1 as the value approaches $V_1 = -\beta V_{\text{CC}}$, i.e.,$V_\text{r}$, when $t = T/2$. Therefore, the period can be obtained as

$$T = 2\frac{C_0 C_\text{p} R_\text{L}}{2C_0 + C_\text{p}} \ln \left[\frac{C_\text{p} + (2C_0 + C_\text{p})\beta}{C_\text{p} - (2C_0 + C_\text{p})\beta} \right] \tag{3.1.10}$$

We would like to note that the oscillation conditions for this topology are governed by the value of parameter β. $V_{1\,\text{down}}(\Delta t)$ has a limiting value $V_{1\,\text{min}}$ when $\Delta t = \infty$. This means that $V_\text{r} = -\beta V_{\text{CC}}$ can not be smaller than $V_{1\,\text{min}}$, otherwise the circuit will not oscillate. This condition can be used to obtain the relation between β and the capacitances C_p and C_0, which is

$$\beta < \frac{C_\text{p}}{2C_0 + C_2} \tag{3.1.11}$$

We need to use this condition so that we can understand the performance limitations of the circuit. Maintaining the values within this range will ensure continuous oscillations and power delivery to the load.
Now, let us find the solution for the power delivered to the load. As we already know the solutions for $V_{2\,\text{down}}(t)$ and $V_{3\,\text{down}}(t)$, the average power can be obtained by substituting them into $P = \frac{2}{T}\int_0^{T/2} (V_{3\,\text{down}}(t) - V_{2\,\text{down}}(t))^2/R_\text{L}\, \text{d}t$, which results in

$$P_{\text{avg}} = \frac{V_{\text{CC}}^2}{R_\text{L}} \frac{2(2C_0 + C_\text{p})\beta}{C_\text{p}} \Big/ \ln \left(\frac{C_\text{p} + (2C_0 + C_\text{p})\beta}{C_\text{p} - (2C_0 + C_\text{p})\beta)} \right) \tag{3.1.12}$$

In the numerator of P_{avg} we again notice the term $V_{\text{CC}}^2/R_{\text{L}}$. Using the concept of P_{r} discussed in Section 2.6, it now equals to

$$P_{\text{r}} = \frac{2(2C_0 + C_{\text{p}})\beta}{C_{\text{p}}} \Big/ \ln\left(\frac{C_{\text{p}} + (2C_0 + C_{\text{p}})\beta}{C_{\text{p}} - (2C_0 + C_{\text{p}})\beta)}\right) \tag{3.1.13}$$

We can observe that this power ratio does not depend on the load resistance R_{L}. Therefore, making the system robust against the load resistance. P_{r} is a function of β and $\rho = C_{\text{p}}/C_0$, which we plot in Figure 3.3.

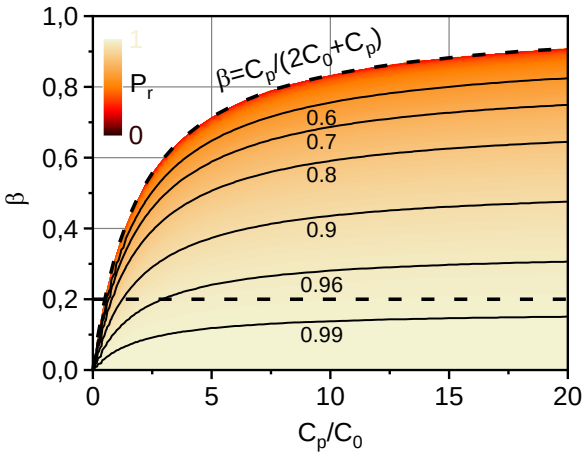

Figure 3.3: Color map of P_{r} as a function of C_{p}/C_0 and β for the self-adaptive WPT.

The dashed line in this figure is defined by the oscillation condition $\beta < C_{\text{p}}/(2C_0+C_2)$. As we can see, oscillations are maintained when this conditions is satisfied. As we move away from the boundary, the power ratio reaches to almost unity for small values of β. This means that the performance of this topology is comparable to the wired case. Also, if the value of β is kept constant, then the system is not sensitive to a change in the large value of C_{p}/C_0, indicating that we can use this configuration for a wide range of capacitances. A change in capacitance in this scenario is equivalent to a change in the transfer distance or the overlap area. We can state that this device, in principle, can transfer energy to any load at any distance and with misalignment as long as the condition defined in 3.1.11 is satisfied.

3.1.1 Analysis when two plate capacitances have different capacitance values

Up to now, we have discussed the case for identical parallel-plate capacitors. But we need to understand how the system will behave when two capacitors have different capacitances. Denoting the capacitance of the parallel-plate capacitor connected to the inverting terminal of the op-amp by $C_{\text{p,left}}$ and the one connected to the output terminal of the op-amp as $C_{\text{p,right}}$, we get the following equations by modifying Equation 3.1.1 for this analysis:

$$C_{\text{p,right}}(V_{\text{out}} - V_3) = C_{\text{p,left}}(V_2 - V_1) \tag{3.1.14}$$

$$V_2 = \frac{C_{\mathrm{p,left}} + C_0}{C_{\mathrm{p,left}}} V_1 \tag{3.1.15}$$

$$C_{\mathrm{p,right}} \frac{d(V_{\mathrm{out}} - V_3)}{dt} = \frac{V_3 - V_2}{R_{\mathrm{L}}} \tag{3.1.16}$$

The initial conditions at $t = 0$ for V_{out} and V_1 are $V_{\mathrm{out}} = -V_{\mathrm{CC}}$ and $V_1 = \beta V_{\mathrm{CC}}$. The voltages V_2 and V_3 change according to the equations defined above. The solutions are found to be

$$V_1(t) = \frac{V_{\mathrm{CC}}}{C_0 + C_{\mathrm{p,left}} + \frac{C_0 C_{\mathrm{p,left}}}{C_{\mathrm{p,right}}}} \left(\left(C_{\mathrm{p,left}} + \left(\frac{C_0 C_{\mathrm{p,left}}}{C_{\mathrm{p,right}}} \right) \beta \right) e^{\frac{-t}{\tau_{\mathrm{gen}}}} - C_{\mathrm{p,left}} \right) \tag{3.1.17}$$

$$V_3(t) = -\frac{V_{\mathrm{CC}}}{C_0 + C_{\mathrm{p,left}} + \frac{C_0 C_{\mathrm{p,left}}}{C_{\mathrm{p,right}}}} \left(\left(C_{\mathrm{p,left}} + \left(\frac{C_0 C_{\mathrm{p,left}}}{C_{\mathrm{p,right}}} \right) \beta \right) e^{\frac{-t}{\tau_{\mathrm{gen}}}} \frac{C_0}{C_{\mathrm{p,right}}} + C_{\mathrm{p,left}} + C_0 \right) \tag{3.1.18}$$

where $\tau_{\mathrm{gen}} = C_0 C_{\mathrm{p,left}} R_{\mathrm{L}} / (C_0 + C_{\mathrm{p,left}} + C_0 C_{\mathrm{p,left}} / C_{\mathrm{p,right}})$. Using these equations, we are able to find the oscillation period

$$T_{\mathrm{gen}} = 2 \frac{C_0 C_{\mathrm{p,left}} R_{\mathrm{L}}}{C_0 + C_{\mathrm{p,left}} + \frac{C_0 C_{\mathrm{p,left}}}{C_{\mathrm{p,right}}}} \ln \left(\frac{C_{\mathrm{p,left}} + \left(C_0 + C_{\mathrm{p,left}} + \left(\frac{C_0 C_{\mathrm{p,left}}}{C_{\mathrm{p,right}}} \right) \right) \beta}{C_{\mathrm{p,left}} - \left(C_0 + C_{\mathrm{p,left}} + \left(\frac{C_0 C_{\mathrm{p,left}}}{C_{\mathrm{p,right}}} \right) \right) \beta} \right) \tag{3.1.19}$$

and the oscillation condition

$$\beta < \frac{C_{\mathrm{p,left}}}{C_0 + C_{\mathrm{p,left}} + \frac{C_0 C_{\mathrm{p,left}}}{C_{\mathrm{p,right}}}} \tag{3.1.20}$$

Then, the generalized power ratio becomes

$$P_{\mathrm{r,gen}} = \frac{2\beta \left(C_0 + C_{\mathrm{p,left}} + \frac{C_0 C_{\mathrm{p,left}}}{C_{\mathrm{p,right}}} \right)}{C_{\mathrm{p,left}}} \Big/ \ln \left(\frac{C_{\mathrm{p,left}} + \left(C_0 + C_{\mathrm{p,left}} + \left(\frac{C_0 C_{\mathrm{p,left}}}{C_{\mathrm{p,right}}} \right) \right) \beta}{C_{\mathrm{p,left}} - \left(C_0 + C_{\mathrm{p,left}} + \left(\frac{C_0 C_{\mathrm{p,left}}}{C_{\mathrm{p,right}}} \right) \right) \beta} \right) \tag{3.1.21}$$

which is referenced to the wired case. With this change, the oscillation period is still a linear function of the load resistance. We plot $P_{\mathrm{r,gen}}$ as a function of $C_{\mathrm{p,left}}/C_0$ and $C_{\mathrm{p,right}}/C_0$ when $\beta = 0.2$, as shown in Figure 3.4.

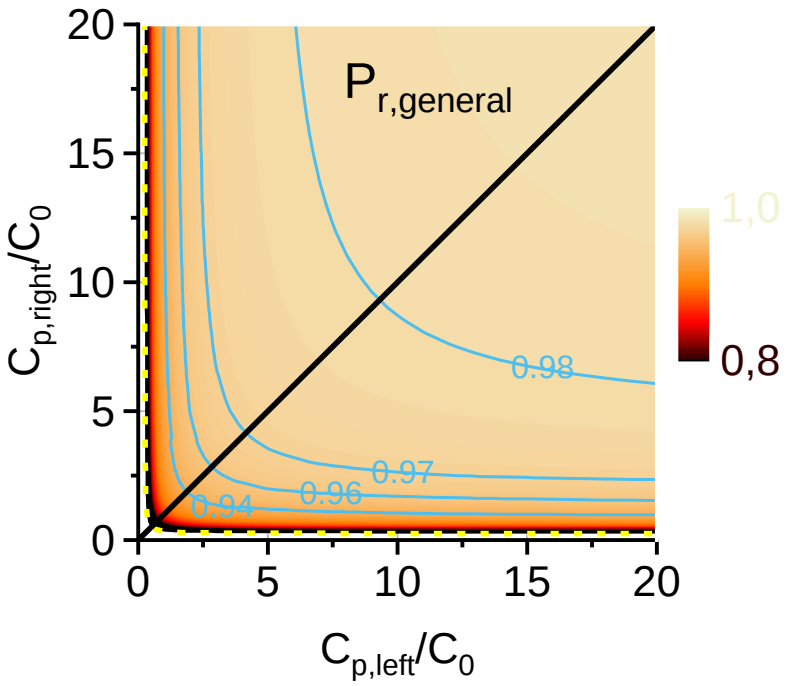

Figure 3.4: Analytical plot of updated power ratio $P_{\mathrm{r,gen}}$ when the plate capacitances are different.

The yellow dashed line represents the boundary condition for oscillation. The black line indicates the behavior when the capacitors have the same capacitance. There is a small change in the power ratio when the parallel-plate capacitors have different values. But, if these capacitance values are greater than C_0, the change in power ratio is small. As a result, this WPT scheme is highly robust against load and wireless link variations.

Our main focus is on the implementation of this WPT scheme. This implementation is robust with respect to change in load and change in capacitance. We will prove that the theoretical model, simulations and experimental results are in good agreement with each other.

3.2 Implementation with Lumped Elements

The experimental setup of the lumped element implementations is shown in Figure 3.5. We have used op-amp TL072IP [36] from Texas Instruments and an oscilloscope to observe the signal at V_{out}, V_3 and V_2. Let us discuss the effect of feedback parameter variations on T and P_{r}.

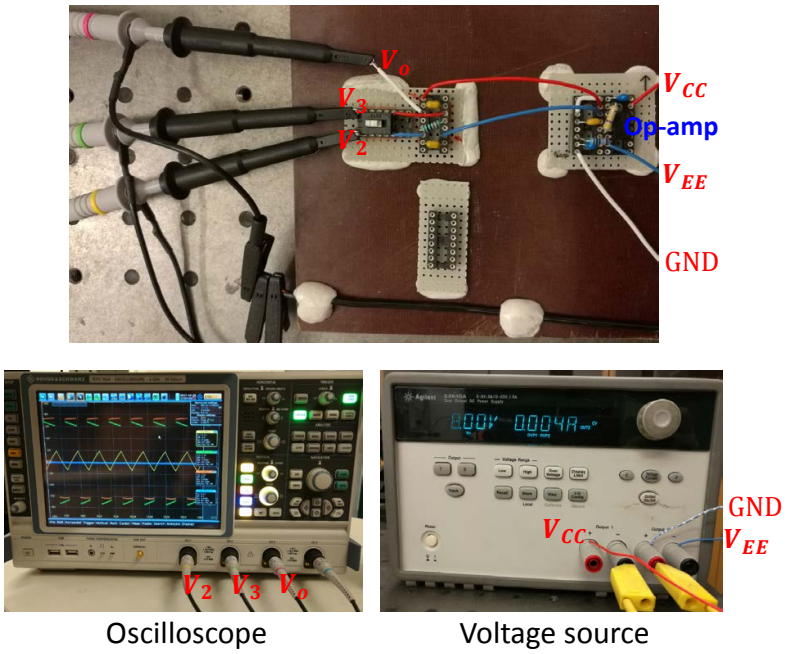

Figure 3.5: Experimental implementation of self-adaptive WPT approach.

3.2.1 Varying system parameter β

We study the effect of β on the oscillating period T and power ratio P_{r}. To do this, we set the source voltage $V_{\mathrm{CC}} = \pm 8\,V$ and load resistance R_{L} to 10 kΩ. We choose three configurations of $\rho = C_{\mathrm{p}}/C_0$ and C_0 as ρ =10 with C_1 =100 nF, $\rho = 2.8$ with C_1 =356 nF and $\rho = 1$ with $C_1 = 1\ \mu$F. The results are presented in Figure 3.6 wherein the symbols represent experimental results and the curves are from the analytical formula 3.1.10 and 3.1.13 from the theoretical section.

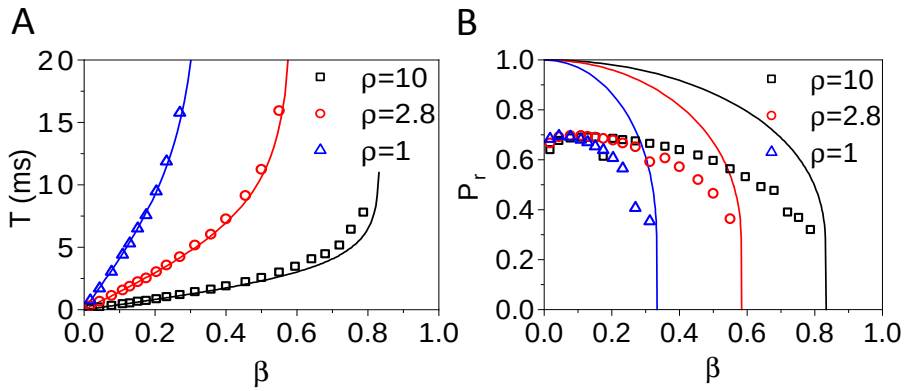

Figure 3.6: Varying β for different ρ and C_1 configurations.

From Figure 3.6 we can see that the experimental results of the power ratio, P_{r} and oscillation period, T agree with the theoretical model, but the P_{r} measured in Figure

3.6 B is smaller than the theoretical value. Less amount of power is delivered to the load due to the voltage drop of the output voltage swing of the op-amp. Taking this drop into consideration, we are able to obtain an alternative power ratio referenced to $P_o = V_o^2/R_L$, where V_o is the amplitude of the actual output of the op-amp. The new P_r is plotted in Figure 3.7 and we can see that the analytical formula and the experimental observations are close to each other.

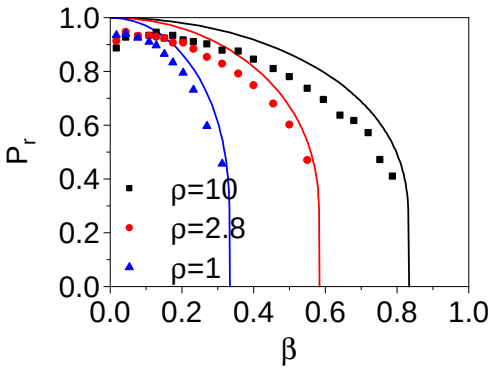

Figure 3.7: Power ratio reference to $P_o = V_o^2/R_L$.

From the figures we can see that smaller values of β give higher power ratio indicating better power delivery to the load. Also, smaller values of β support a wider range of capacitances. These conclusions are consistent with the analytic results. From this fact we are able to conclude that a small value of β is ideal for this implementation.

3.2.2 Varying load resistance R_L

Now, let us study the performance of the system while we change the load resistance R_L. To do this, we set the value of $\beta = 0.2$ and define $\rho = 10$ with C_1 =100 nF and $\rho = 2.8$ with $C_1 = 356$ nF. The results are plotted in Figure 3.8. The symbols denote the experimental values of T and P_r whereas the solid lines depict the analytical solutions.

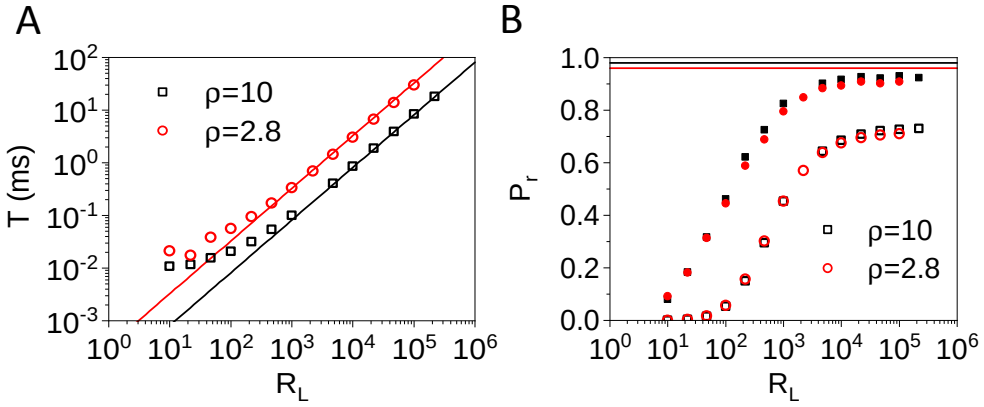

Figure 3.8: Oscillation period T and power ratio P_r on the load when varying R_L for different ρ and C_1 configurations.

We can see from the results that T follows the theoretical solution for large values of the load resistance but it deviates from the theoretical solution when T is around $T = 10^{-2}$ ms. The small values of load resistances decreases the operating period of the system leading to issues arising from the finite slew rate of the op-amp. This limits the performance of the system in terms of power delivery at low loads. Therefore, while the theoretical values of the power ratio are 0.98 and 0.96 respectively for the chosen configurations, this practical limitation affects the system, as we can observe in Figure 3.8 B that P_r drops at lower resistance values. The next step for this work is to study the robustness of this system with respect to changes in capacitance and implementing the wireless link with parallel-plate capacitors.

3.3 Implementation with Parallel Plates

The preliminary implementation of the circuit was done using copper plates. While implementing with metallic plates we have to take precaution to prevent the two plates from shorting. This was avoided by the use of paper between the two plates and the capacitance was calculated using the dielectric constant of 1.8 as shown in Figure 3.9.

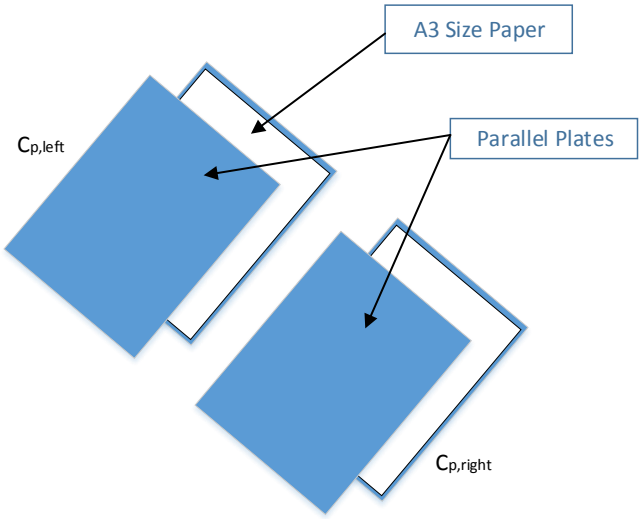

Figure 3.9: Practical implementation of parallel-plate capacitors.

The proof of concept design was implemented with copper plates of dimensions 50 cm × 30 cm. We were able to transmit power wirelessly. This is indicated by the glowing of LEDs in series with the load resistance. Here, the boundary of the oscillation regime is defined as the moment at which the LEDs stop glowing. However, as the copper plates are very flexible and not flat, the distance between the two plates is not uniform, resulting in hard control of the capacitance values. Therefore, we moved onto an implementation with aluminum plates which have flat surfaces. We provide a more extensive analysis of the aluminum plate implementation.

3.3.1 Experimental demonstration with aluminum plates

In this section, we discuss the implementation of the WPT system with aluminum plates. The op-amp used here is TL051CP [37] from Texas Instruments. The system parameters are $R_1 = 3.9$ MΩ, $R_2 = 1$ MΩ, $C_0 = 4.7$ nF and $V_{CC} = \pm$ 12 V. The wireless link is realized using aluminum plates of length 50 cm × width 30 cm. The separation between the plates $d = 0.1$ mm provides the plate capacitance in nF range. We measure V_{out}, V_2 and V_3 with the help of a four channel oscilloscope. We process data to determine the oscillation frequency and the power ratio. Here, we will discuss the robustness of the system with respect to changes in the load resistance R_L and plate position which determines the capacitance. We should keep in mind that the plate position represents the WPT link in which the two plates behave as a transmitter and a receiver. When we are changing the location of the receiver, the capacitances of the parallel-plate capacitors change. The experimental setup is shown in Figure 3.10 A.

We will first discuss the robustness of the system with respect to changes in load resistance R_L. The capacitance is measured to be 18.1 nF. From the theory, we know that the system should work for all values of load resistances. However, the op-amp used for proving the concept has a physical limitation (slew rate) on the working frequency which limits the lowest load to be 400 Ω.The closest available value for a resistor above 400 Ω is 470 Ω in our lab. Therefore we are able to vary the resistance from 470 Ω to 4.7 MΩ. The results obtained are shown in Figures 3.10 B and 3.10 C.

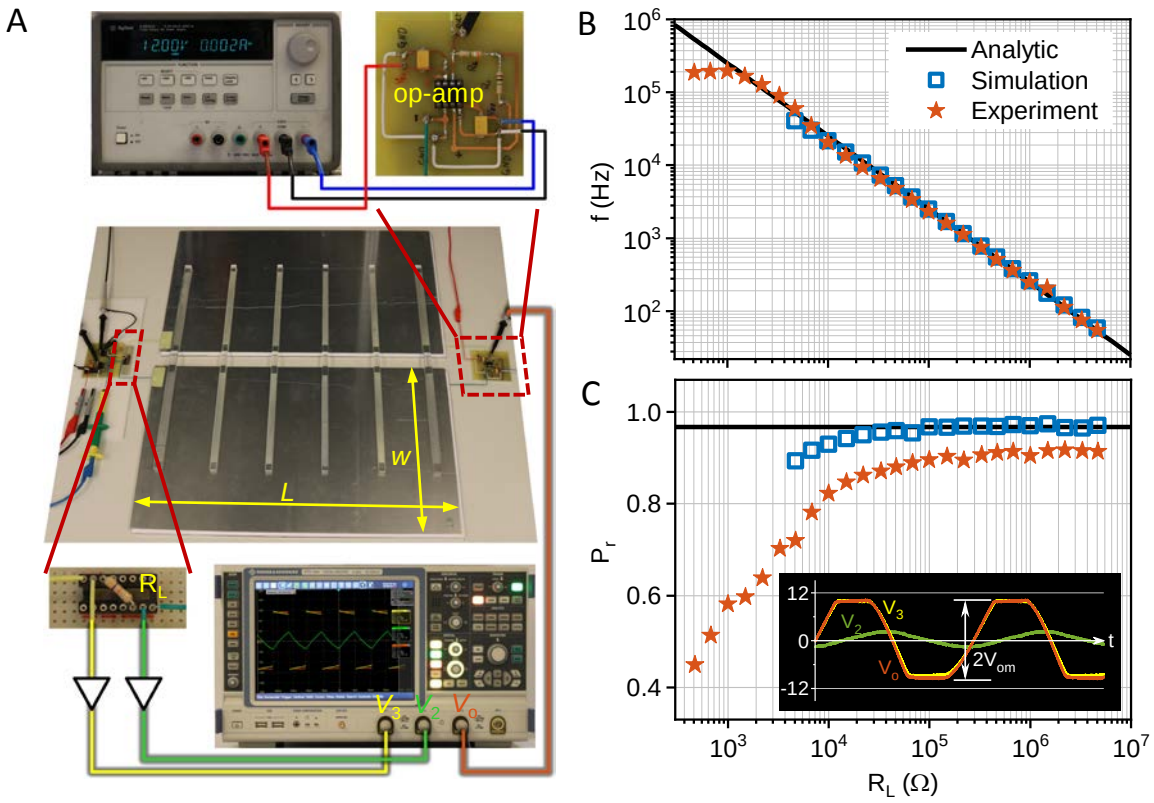

Figure 3.10: Experimental setup and robustness against changes in load resistance R_{L}.

It is observed that the simulation and experimental values of the frequency acknowledge each other. Referring to Equation 3.1.10, frequency is inversely proportional to R_{L} as $f = 1/T$, and the analytical solution is denoted by the solid black line in Figure 3.10 B. In Figure 3.10 C, we can see that the power ratio P_{r} at lower load resistances do not follow the analytical solution. This discrepancy is a result of the finite slew rate of the op-amp. In this case, we see that the slew rate limitation prohibits the output from changing its state instantly as shown in the inset of Figure 3.10 C. Also, we can see that the output voltage swing is less than $\pm V_{\mathrm{CC}}$. Therefore, in order to give a more reasonable power ratio, we need to make certain changes to the formula. The formula for power ratio is given by $P_{\mathrm{r}} = P_{\mathrm{avg}}/P_0$, taking the decreased output voltage swing into the picture, the formula changes to $P'_{\mathrm{r}} = P_{\mathrm{avg}}/P'_0$ where $P'_0 = V_{\mathrm{m}}^2/R_{\mathrm{L}}$ and $2V_{\mathrm{m}}$ is the measured peak to peak voltage of the output. As we can see in 3.10 C, the measured and simulated power ratios agree well with the analytical values except for low values of R_{L}.

In all measurements, we have used buffer circuits made with the same op-amp. These are represented by triangles connected to the oscilloscope, as shown in Figure 3.10 A.

Now, we shall demonstrate the robustness of the system with respect to the changes

in capacitance, i.e., change in the receiver position. We change the overlap of the two plates by sliding the top plate as shown in the inset of Figure 3.11 A. C_p is a linear function of the overlap distance l and in the implementation we change the overlap from 10 cm to 50 cm. The measured frequencies and power ratios are shown in 3.11 B and 3.11C for five load values of 1 kΩ, 3.3 kΩ, 10 kΩ, 33 kΩ and 100 kΩ.

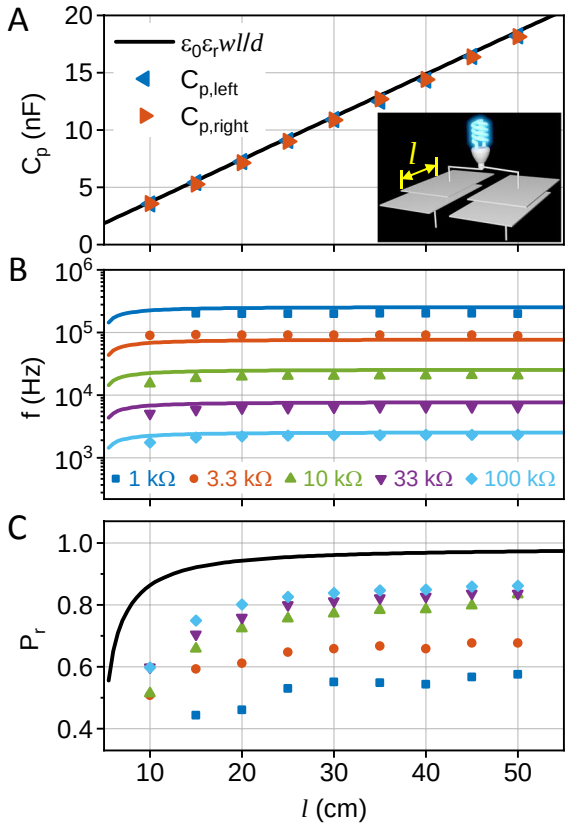

Figure 3.11: Experimental demonstration of robustness against receiver position.

It can be seen from Figure 3.11 that the WPT system operates robustly for changes in the receiver position. For a fixed load, the working frequency is almost constant, while the power ratio increases due to the change in the overlap distance. In experimentation we have also demonstrated that misalignment of the parallel plates does not affect the WPT operation. From these discussions we conclude that the theory is validated with the experimental results.

In this system, there is no inevitable loss in the output resistance of the generator as this output resistance is the load itself. The dissipation losses in R_1 and R_2 are negligible and parasitic losses occur only in the op-amp (or any switching component in the circuit) which are present in all conventional systems as well. The conventional definition of WPT efficiency is the ratio of power delivered to the load and the output of the generator. But in our case, the efficiency under the conventional definition is always 100%. The overall efficiency is the correct parameter to measure the efficiency of these systems. Overall efficiency is defined as the ratio of power

consumption in the load to that of the total power taken from the DC source, i.e., $\eta = P_{\text{avg}}/P_{\text{in}}$. For this experiment, we achieved the maximum overall efficiency of 36.7 %. Low overall efficiency can be related to the comparable large losses occurring in the op-amp. This discussion is illustrated in Figure 3.12, which shows the overall efficiency analysis for different load resistances.

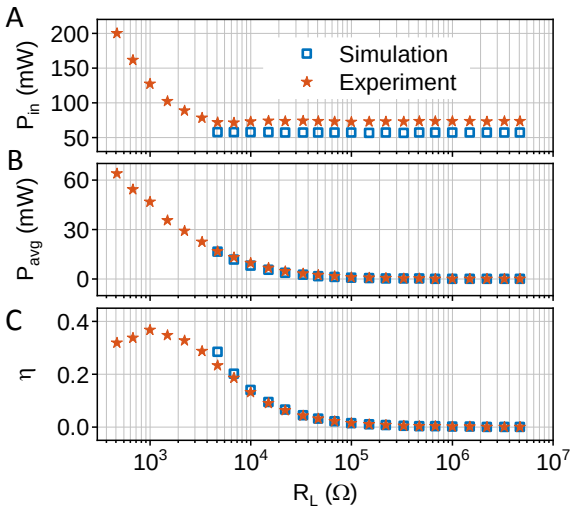

Figure 3.12: Overall efficiency analysis for different load resistances.

Next, we compare the new WPT system to conventional WPT systems. We can see why the proposed system performs better. For the power ratio P_{r}, it is load-independent in the proposed WPT system, whereas in the conventional WPT systems, it is load-dependent. This load dependence decreases the power delivery at small load values. This can be seen in Figure 3.13 which shows the analytical results of the two power ratios with respect to the load. The conventional P_{r} here is plotted with parameters $C_{\text{p}} = 18.1$ nF, $C_0 = 4.7$ nF, $R_{\text{f}} = 100$ kΩ, and $\beta = 0.2$ ($R_1 = 1$ MΩ, $R_2 = 3.9$ MΩ).

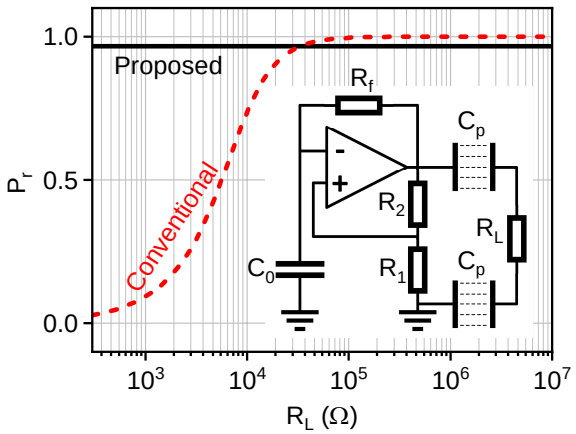

Figure 3.13: Comparison of power ratio P_r between conventional and proposed WPT systems. The conventional WPT system is discussed in Section 2.6 and it is schematically shown in inset.

3.4 Another Location for WPT Unit

In Section 2.7, we introduced two possibilities for integrating the WPT unit in an RC oscillator. In this section, we discuss the other possibilities where the WPT receiver is placed in the place of C_0 and the circuit looks as shown in Figure 3.14.

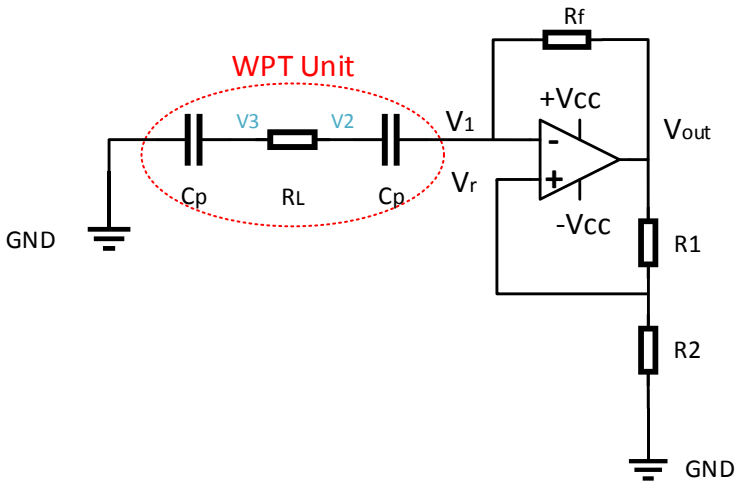

Figure 3.14: Circuit diagram for another location of the WPT reception unit.

The analytical solution of this system can be derived using Kirchoff's laws and Equations 2.5.1 and 2.5.2. The feedback path of this topology is through the feedback resistor R_f. At junction V_1, the current i flowing through the feedback path

of the op-amp flows towards the WPT unit. We have the following equations:

$$i = \frac{V_{\text{out}} - V_1}{R_{\text{f}}} = C_{\text{p}} \frac{\text{d}(V_1 - V_2)}{\text{d}t} = \frac{V_2 - V_3}{R_{\text{L}}} = C_{\text{p}} \frac{\text{d}V_3}{\text{d}t} \tag{3.4.1}$$

These are the master equations and the initial conditions can be found from Figure 3.15 which is from LTSpice simulation. V_{out} is shown by the green curve and V_1 is shown by the blue curve. V_2 and V_3 have very small difference due to the small current and here we only show V_2 by the red waveform.

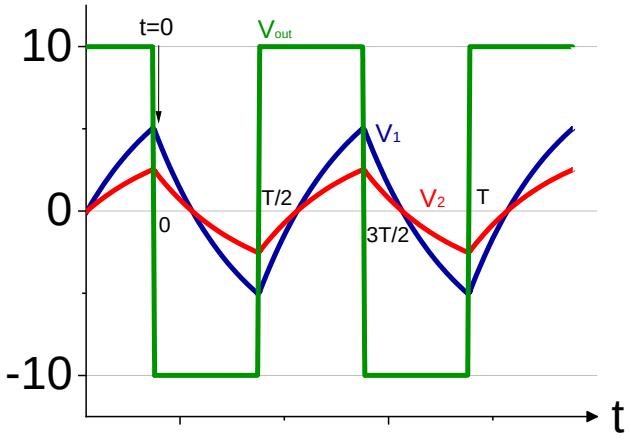

Figure 3.15: Voltage oscillations for the other approach.

The circuit was implemented using $R_{\text{f}} = 180$ kΩ and β =0.5 ($R_1 = R_2 = 10$ kΩ). The plate dimensions are 10 cm × 10 cm with a gap of 1.5 mm, allowing the capacitance to be approximately 100 pF. The frequency of operation in both simulation and experimentation is 10 kHz. Even though the circuit theoretically is a self-oscillating circuit for WPT, it has several limitations for optimal power delivery to the load. Firstly, insufficient current is being delivered to the WPT unit, as this current is not only limited by the load resistor R_{L} but also by feedback resistor R_{f}. In addition, we need a larger R_{f} in order to maintain oscillations in the circuit. This is again due to the limitation caused by the slew rate of the op-amp. If we decrease the value of R_{f}, then the frequency of operation increases. This increase may drive the op-amp to its limiting case. Secondly, the maximum voltage V_2 can reach is equal to V_1. This voltage is limited by parameter β of the circuit which in our case is 0.5. Increasing the value of beta may terminate the oscillation as R_{f} occupies a certain voltage. Even when β increases within the working range, the delivered power will not improve much as V_2 and V_3 are very close to each other. As a result, the average power delivered to the load is smaller making this option less interesting for further analysis.

In this chapter, we discussed in detail the self-adaptive WPT approach. We introduced the theory required for the implementation of such a system followed by the experimental analysis. We can conclude that the experimental, theoretical and simulation results are in good agreement with each other.

4 Alternative Design based on Colpitts Oscillator

Theoretically, there are many possibilities to make WPT systems from self-oscillating circuits. Here, we provide an alternative WPT design based on the Colpitts oscillator. The Colpitts oscillator is one of the many oscillators used to implement a resonant WPT system using an op-amp for our integrated system concept. A Colpitts oscillator consists of two capacitors and an inductor to determine the tank circuit.

4.1 Circuit Design

A conventional Colpitts oscillator can be transformed to a WPT system by substituting one of the capacitors in the tank circuit by the WPT unit, as shown in the schematic in Figure 4.1 A. This oscillator uses a capacitive voltage divider network as the feedback source. This satisfies the necessary condition for our approach which states that the WPT unit should be introduced in the feedback network of the circuit. We cannot substitute the WPT unit in the position of C' because C' is not a part of the feedback loop for the circuit. This transition can be observed in Figure 4.1 A. The implementation of the oscillator using lumped elements is shown in Figure 4.1 B and is discussed here. For this implementation, we simply use lumped capacitors C instead of parallel-plate capacitors. For a simple demonstration, we used lumped elements with values $R_{\mathrm{f}} = 2.2\,\mathrm{M\Omega}$, $R_1 = 220\,\Omega$, $L = 100$ mH, and $C' = 470$ nF.

4.2 Analytical Results

The analytical formulas for the frequency of operation and power delivered to the load are as follows:

$$f = \frac{1}{2\pi\sqrt{LC_{\mathrm{T}}}} \tag{4.2.1}$$

$$P_{\mathrm{avg}} = \frac{1}{RT}\int_0^T \Delta V^2 \mathrm{d}t \tag{4.2.2}$$

where, C_{T} is the total series capacitance and ΔV is the voltage drop across the load. We study the oscillation period and the power consumption by the load with different load resistances R and capacitances C (modeling possibly varying loads and wireless transfer distances).

4.3 Experimental Results

The black and red curves in Figure 4.1 C (values close to each other) show the voltages at the two ends of the load when $R = 1\,\Omega$ and $C = 470$ pF. With this capacitance value, we are modeling the power transfer between two metal plates with dimensions of 50 cm $\times$ 50 cm and separation of 4.71 mm. It can be seen that quasi-sinusoidal oscillations are created at the load and the oscillation period is T $\approx 32\ \mu$s. The power delivered to the load is measured to be 2.4mW. However, the overall efficiency is low as the total power supplied from the DC source equals 375 mW. There are two main reasons for this high power consumption in the circuit.

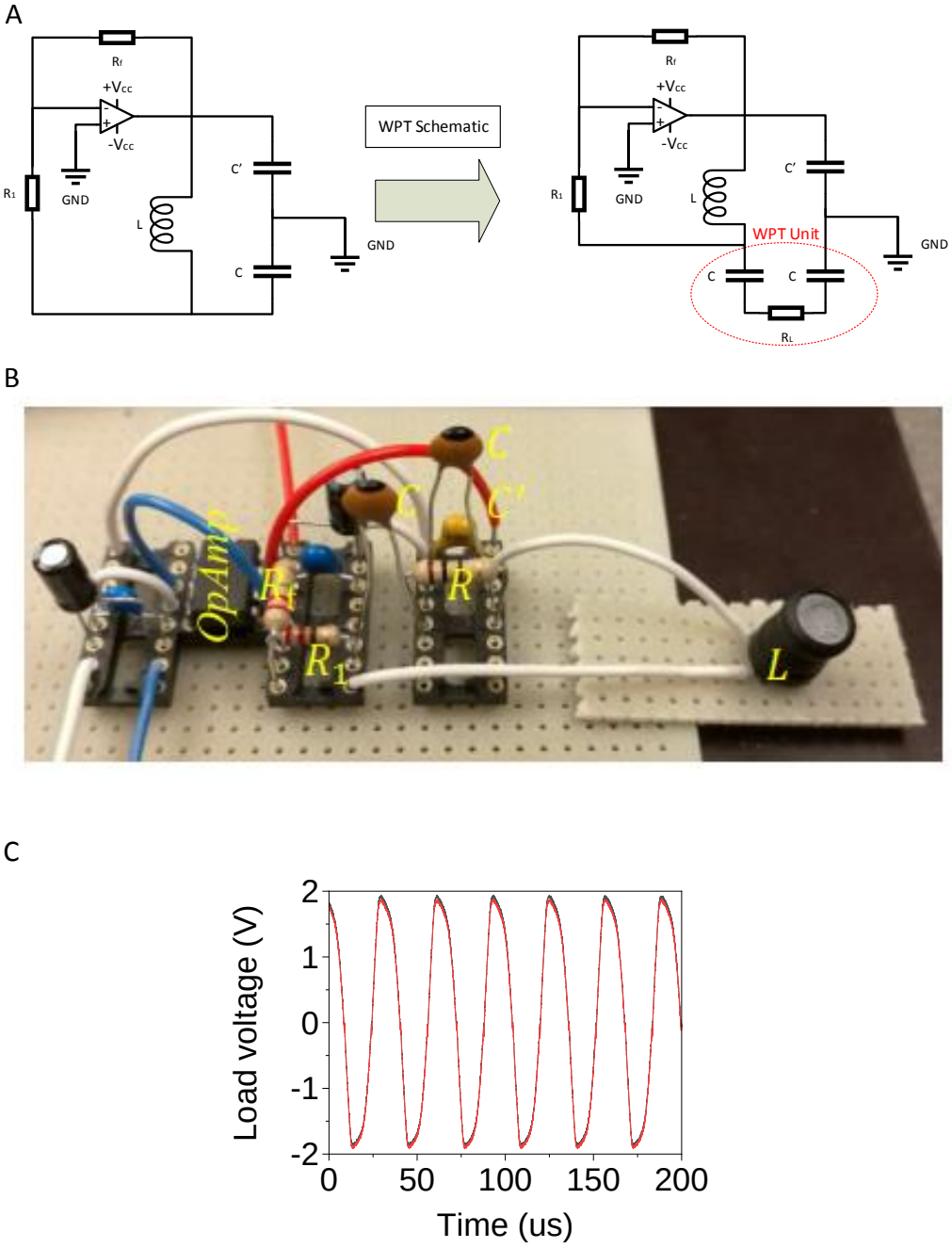

Figure 4.1: (A) Implementation of WPT system by modifying Colpitts oscillator. (B) Experimental setup. (C) Measured load voltage oscillation.

One is the chosen op-amp [38] which consumes a significant amount of energy. The other reason is that the chosen topology of the self-oscillating circuit, in which the capacitor C' directly connects the output of the amplifier to the ground. As the output is an oscillating wave, there is a non-negligible AC current passing through C' to the ground, leading to high power loss in the output resistance of the amplifier.

We note that the power consumption by the other lumped elements (R_{f}, R_1, L and C) is very low as compared to the load resistance. Therefore, the overall efficiency of this WPT system based on self-oscillating circuit can be improved by using a better amplifier and alternative topologies of self-oscillating circuits, such as the one discussed in the previous chapter.

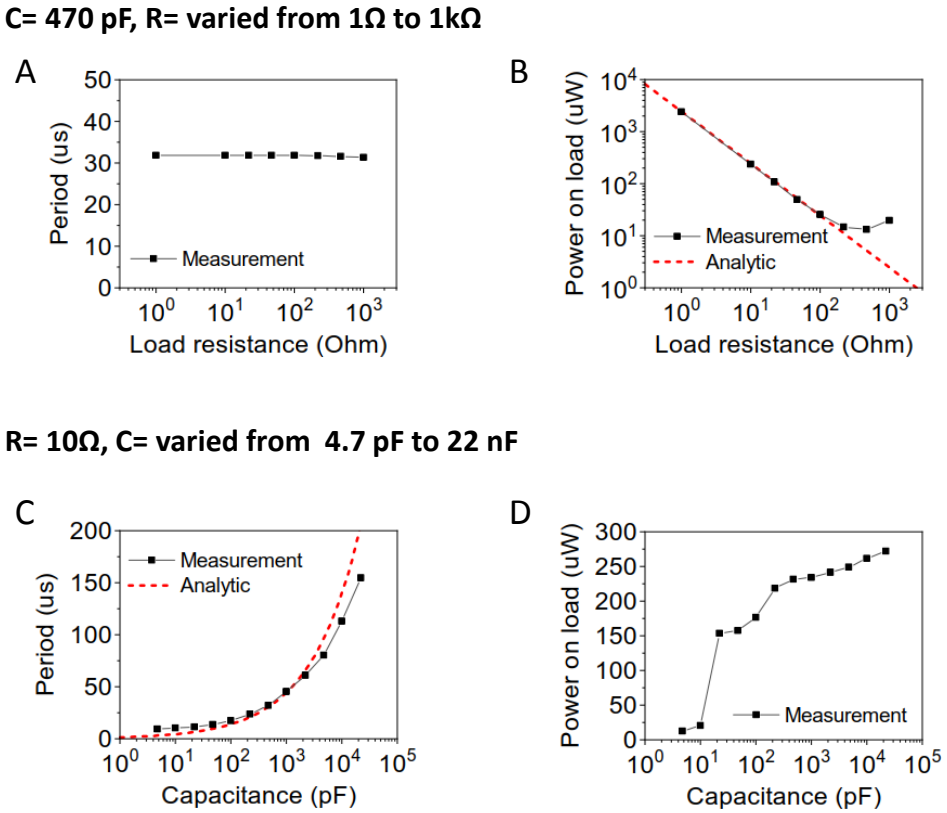

Figure 4.2: Experimental results of the WPT system based on the Colpitts oscillator.

Next, we perform the same measurements for different load resistances while keeping $C = 470$ pF which signifies a fixed distance to the load. The measured oscillation period and power delivery for different load R are shown in Figures 4.2 A and 4.2 B. It is clear that the period exhibits remarkable stability with respect to R which admits operation at a fixed frequency with a changing load. We see that the wireless system creates a virtual nearly-ideal voltage source at the load position, and the power consumption at the load decreases as $1/R$ when $R \leq 220\ \Omega$ simply because the oscillating voltage across R is almost unchanged. When $R > 220\ \Omega$, the electromotive force at the load increases. The red dashed curve in Figure 4.2 B is the plot of $\frac{1}{2}\Delta V_{\mathrm{max}}^2/R_{\mathrm{L}}$ with $\Delta V_{\mathrm{max}} = 70$ mV, showing that the WPT system indeed realizes a nearly ideal voltage source at the load position, for load resistances smaller than 220 Ω. Finally, we study the power transfer when we vary the capacitance value C, corresponding to changes of the transfer distance in actual WPT implementations. In this case, we keep the load resistance constant at $R = 10\ \Omega$ and change

the capacitance values from 4.7 pF to 22 nF (i.e., corresponding to changes of the wireless transfer distance from 0.471 m to 0.1 mm for capacitors realized based on metal plates with area 50×50 cm^2). The experimental results are shown in Figures 4.2 C and 4.2 D. As we observe, the oscillation period increases when we increase C. Actually, the self-oscillation period can be obtained by analyzing the tank circuit, which gives $T = 2\pi\sqrt{LCC'(C + 2C')}$ according to Equation 4.2.1. This analytical period is plotted as the red dashed curve, explaining the experimental results. On the other hand, the power delivered to the load increases as the capacitance gets larger which corresponds to the decrease in distance of the plates. It is due to the fact that a larger capacitance supports more charge accumulation inside the capacitor leading to a higher voltage drop across the load. The aforementioned results clearly show that this version of the proposed self-oscillating WPT systems is robust against changes of the load and the receiver resistance (transfer distance).

In this chapter, we discussed an alternative method for realizing self-oscillating WPT system using a Colpitts oscillator. With these results, we can say that this concept is not limited to a single circuit design. Of course, this concept can be realized using other circuits as well and we are further exploiting this paradigm.

5 Conclusions

We have presented a new paradigm for wireless power transfer, wherein the transformation of DC or supply voltage into microwave oscillations is integrated with the WPT unit. The microwave energy is directly produced at the load. Both conventional and proposed systems contain a microwave generator which consumes some energy. But, the proposed system consists of only a generator, whereas the conventional systems have certain parasitic losses due to the additional circuitry. The proposed paradigm automatically adapts itself to changes in receiver position and load variations. Hence, it avoids the need of additional tuning that is required in the conventional resonating WPT systems. As a result, the robustness of power transfer is improved in the new paradigm. The proposed on-site WPT scheme based on the self-oscillating concept realizes a virtual, nearly ideal voltage source at the position of the power-receiving load. In one particular design, this voltage source is comparable to the wired case under certain conditions, resulting in efficient wireless power transfer. A maximum overall efficiency of 36.7% is obtained.

We have presented and discussed the theoretical analysis and experimental implementation of the WPT systems within this new paradigm. It can be seen that these results are very distinct from the conventional designs, which have limited working frequency range for good performance and require dynamic adjustment for maintaining matching (for optimal operation). To improve the current design we can work with different dielectrics in between the metallic plates (to increase the capacitance) and improve the power transfer. For example, underwater WPT is an interesting application for the proposed system. The use of water (very high permittivity) as a dielectric improves the amount of power that can be transmitted and/or reduces the size of the metal plates. This improves the design from the mechanical as well as the electronics perspective as we have smaller plate size and improved power transfer.

The performance of the realized WPT systems discussed in this thesis can be improved by using better and faster op-amps. Also, different oscillator circuit topologies can be developed to achieve better self-oscillating WPT systems. Moreover, this concept can be realized with transistor configurations such as using class E oscillator circuits.

References

[1] N. Tesla, "Apparatus for transmitting electrical energy," U. S. Patent 1 119 732, Dec., 1914.

[2] W. C. Brown, "The history of power transmission by radio waves," *IEEE Trans. Microwave Theory Tech.*, vol. 32, no. 9, pp. 1230–1242, Sep. 1984.

[3] W. C. Chao, "Battery charging device for mobile phone," U. S. Patent US6 057 668A, 2000.

[4] D. M. Vilathgamuwa and J. P. K. Sampath, "Plug in electric vehicles in smart grids," *Springer Singapore*, pp. 33–60, Nov. 2015.

[5] M. Kakegawa, "Apparatus for transmitting energy to a device implanted in a living body," U. S. Patent US4 432 363A, 1984.

[6] J. S. Ho, A. J. Yeh, E. Neofytou, S. Kim, Y. Tanabe, B. Patlolla, R. E. Beygui, and A. S. Y. Poon, "Wireless power transfer to deep-tissue microimplants," *Proceedings of the National Academy of Sciences*, vol. 111, no. 22, pp. 7974–7979, May 2014.

[7] David M. Pozar, *Microwave Engineering*. Wiley, 2012.

[8] G. D. D. Christopher R. Valenta, "Harvesting wireless power," *IEEE Microw. Mag.*, vol. 15, no. 4, pp. 108–120, Jun. 2014.

[9] T. Y. Kheng, *Energy Harvesting Autonomous Sensor Systems: Design, Analysis, and Practical Implementation*. CRC Press, 2013.

[10] S. Y. R. Hui, W. Zhong, and C. K. Lee, "A critical review of recent progress in mid-range wireless power transfer," *IEEE Trans. Power Electron.*, vol. 29, no. 9, pp. 4500–4511, Sep. 2014.

[11] A. Kurs, A. Karalis, R. Moffatt, J. D. Joannopoulos, P. Fisher, and M. Soljacic, "Wireless power transfer via strongly coupled magnetic resonances," *Science*, vol. 317, no. 5834, pp. 83–86, Jul. 2007.

[12] A. Alphones and P. Jayathurathnage, "Review on wireless power transfer technology (invited paper)," in *2017 IEEE Asia Pacific Microwave Conference (APMC)*. IEEE, Nov. 2017.

[13] S. Aldhaher, P. C.-K. Luk, A. Bati, and J. F. Whidborne, "Wireless power transfer using class e inverter with saturable DC-feed inductor," *IEEE Trans. Ind. Appl.*, vol. 50, no. 4, pp. 2710–2718, Jul. 2014.

[14] K. E. Koh, T. C. Beh, T. Imura, and Y. Hori, "Impedance matching and power division using impedance inverter for wireless power transfer via magnetic resonant coupling," *IEEE Trans. Ind. Appl.*, vol. 50, no. 3, pp. 2061–2070, May 2014.

[15] J. Dai and D. C. Ludois, "A survey of wireless power transfer and a critical comparison of inductive and capacitive coupling for small gap applications," *IEEE Trans. Power Electron.*, vol. 30, no. 11, pp. 6017–6029, Nov. 2015.

[16] Y. Zhang, Z. Zhao, and K. Chen, "Frequency-splitting analysis of four-coil resonant wireless power transfer," *IEEE Trans. Ind. Appl.*, vol. 50, no. 4, pp. 2436–2445, Jul. 2014.

[17] S. R. Cove and M. Ordonez, "Wireless-power-transfer planar spiral winding design applying track width ratio," *IEEE Trans. Ind. Appl.*, vol. 51, no. 3, pp. 2423–2433, May 2015.

[18] S. Y. Hui, "Planar wireless charging technology for portable electronic products and qi," *Proc. IEEE*, vol. 101, no. 6, pp. 1290–1301, Jun. 2013.

[19] G. A. Covic and J. T. Boys, "Modern trends in inductive power transfer for transportation applications," *IEEE Journal of Emerging and Selected Topics in Power Electronics*, vol. 1, no. 1, pp. 28–41, Mar. 2013.

[20] D. Rozario, N. A. Azeez, and S. S. Williamson, "A modified resonant converter for wireless capacitive power transfer systems used in battery charging applications," in *2016 IEEE Transportation Electrification Conference and Expo (ITEC)*. IEEE, Jun. 2016.

[21] A. P. Hu, C. Liu, and H. L. Li, "A novel contactless battery charging system for soccer playing robot," in *2008 15th International Conference on Mechatronics and Machine Vision in Practice*. IEEE, Dec. 2008.

[22] H. Zheng, K. Tnay, N. Alami, and A. P. Hu, "Contactless power couplers for respiratory devices," in *Proceedings of 2010 IEEE/ASME International Conference on Mechatronic and Embedded Systems and Applications*. IEEE, Jul. 2010.

[23] M. Budhia, G. A. Covic, and J. T. Boys, "Design and optimization of circular magnetic structures for lumped inductive power transfer systems," *IEEE Trans. Power Electron.*, vol. 26, no. 11, pp. 3096–3108, Nov. 2011.

[24] Z. Dang and J. A. A. Qahouq, "Modeling and investigation of magnetic resonance coupled wireless power transfer system with lateral misalignment," in *2014 IEEE Applied Power Electronics Conference and Exposition - APEC 2014*. IEEE, Mar. 2014.

[25] F. Kong, "Coil misalignment compensation techniques for wireless power transfer links in biomedical implants," Master's thesis, Graduate School—New Brunswick Rutgers, The State University of New Jersey, 2015.

[26] A. P. Sample, D. A. Meyer, and J. R. Smith, "Analysis, experimental results, and range adaptation of magnetically coupled resonators for wireless power transfer," *IEEE Trans. Ind. Electron.*, vol. 58, no. 2, pp. 544–554, Feb. 2011.

[27] P. K. S. Jayathurathnage, A. Alphones, and D. M. Vilathgamuwa, "Optimization of a wireless power transfer system with a repeater against load variations," *IEEE Trans. Ind. Electron.*, vol. 64, no. 10, pp. 7800–7809, Oct. 2017.

[28] Y. Luo, Y. Yang, and Z. Chen, "Self-tuning wireless power transmission scheme based on on-line scattering parameters measurement and two-side power matching," *Sci. Rep.*, vol. 4, no. 1, Apr. 2014.

[29] D. S. Ricketts, M. J. Chabalko, and A. Hillenius, "Optimization of wireless power transfer for mobile receivers using automatic digital capacitance tuning," in *2013 European Microwave Conference*, Oct. 2013.

[30] S. Assawaworrarit, X. Yu, and S. Fan, "Robust wireless power transfer using a nonlinear parity-time-symmetric circuit," *Nature*, vol. 546, no. 7658, pp. 387–390, Jun. 2017.

[31] Y. Ra'di, B. Chowkwale, C. A. Valagiannopoulos, F. Liu, A. Alu, C. R. Simovski, and S. A. Tretyakov, "On-site wireless power generation," *IEEE Trans. Antennas Propag.*, vol. 66, no. 8, pp. 4260–4268, Aug. 2018.

[32] S. A. Tretyakov, C. R. Simovski, C. A. Valagiannopoulos, and Y. Ra'di, "Self-oscillating wireless power transfer systems," arXiv: 1705.00533v1, 2017.

[33] F. Liu, B. Chowkwale, P. Jayathurathnage, and S. Tretyakov, "Robust wireless power transfer: A self-adaptive approach," arXiv: 1806.09438, 2018.

[34] B. Carter and R. Mancini, *Op Amps for Everyone*. Newnes, 2009.

[35] "Predicting op amp slew rate limited response," Texas Instruments, Oct. 2002. [Online]. Available: http://www.ti.com/lit/an/snoa852/snoa852.pdf

[36] "Tl07xx low-noise JFET-input operational amplifiers," Texas Instruments, Sep. 2017. [Online]. Available: http://www.ti.com/lit/ds/symlink/tl072.pdf

[37] "Tl05x,tl05xa enhanced-JFET low offset operational amplifiers," Texas Instruments, Feb. 2003. [Online]. Available: http://www.ti.com/lit/ds/symlink/tl051a.pdf

[38] "LM7171 very high speed, high output current, voltage feedback amplifier," Texas Instruments, Sep. 2014. [Online]. Available: http://www.ti.com/product/LM7171/technicaldocuments